Resolving Convection of CO2 Ice Clouds in the Martian Polar Nights

Vincent Caillé, Aymeric Spiga, Anni Määttänen, Lola Falletti, Christophe Mathé

Geophysical Research Letters

RESEARCH LETTER
10.1029/2023GL106923

Resolving Convection of CO_2 Ice Clouds in the Martian Polar Nights

Vincent Caillé[1], Aymeric Spiga[2], Anni Määttänen[1], Lola Falletti[1], and Christophe Mathé[3]

[1]LATMOS/IPSL, Sorbonne Université, UVSQ Université Paris-Saclay, CNRS, Paris, France, [2]Laboratoire de Météorologie Dynamique/Institut Pierre Simon Laplace (LMD/IPSL), Sorbonne Université, Centre National de La Recherche Scientifique (CNRS), École Polytechnique, École Normale Supérieure (ENS), Paris, France, [3]LESIA, Observatoire de Paris, Université PSL, CNRS, Sorbonne Université, Université Paris Cité, Meudon, France

Key Points:

- Coupling a convection model with a CO_2 microphysics scheme can simulate the formation of convective CO_2 ice clouds triggered by realistic perturbations
- These is a strong coupling between CO_2 ice cloud convection and dust cycle in the troposphere
- The convective process intensity depends strongly on the number of available condensation nuclei and the temperature of the perturbation

Correspondence to:
V. Caillé,
vincent.caille@latmos.ipsl.fr

Citation:
Caillé, V., Spiga, A., Määttänen, A., Falletti, L., & Mathé, C. (2024). Resolving convection of CO_2 ice clouds in the Martian polar nights. *Geophysical Research Letters*, *51*, e2023GL106923. https://doi.org/10.1029/2023GL106923

Received 20 OCT 2023
Accepted 22 APR 2024

Abstract Martian CO_2 ice clouds are intriguing features, representing a rare occurrence of atmospheric condensation of a major component. These clouds play a crucial role due to their radiative properties, interactions with surface, and coupling with microphysical cycles of aerosols. Observations have been limited, prompting modeling studies to understand their formation and dynamics. Here, we present the first high-resolution 3D simulations of CO_2 ice clouds using a Large-Eddy Simulation (LES) model incorporating CO_2 microphysics. We investigate cloud formation in idealized temperature perturbations in the polar night. A reference simulation with a −2K perturbation demonstrates that the formed CO_2 ice cloud possesses a convective potential, leading to its ascent in the troposphere. We determine the timescales and orders of magnitude of various phenomena involved in the lifecycle of a CO_2 ice cloud. Sensitivity tests show that convection can be inhibited or intensified by the thermodynamic and microphysical conditions of the simulated environment.

Plain Language Summary CO_2 ice clouds have been observed in the Martian polar nights in the lower atmosphere. These clouds are extremely challenging to observe due to the lack of sunlight. However, they play a significant role in Mars' climate, especially through interactions with the surface and other atmospheric species. To study the formation processes of these clouds, we use a high-resolution model. Even a relatively weak cooling can lead to the formation of a CO_2 ice cloud with convective potential, enabling it to move vertically upward. We determine the characteristic times and altitudes of this phenomenon and investigate how they respond when atmospheric parameters, such as cooling temperature, the presence of extra dust, or horizontal winds are varied. Our findings show that some of these parameters can either inhibit or enhance convection development.

1. Introduction

CO_2 is the overwhelmingly dominant component of the Martian atmosphere, with an estimated abundance of nearly 96% (Mahaffy et al., 2013). In this regard, CO_2 ice clouds are particularly interesting objects as they represent one of the rare occurrences of atmospheric condensation of a major component. Furthermore, these clouds play a crucial role in the atmosphere due to their radiative properties and their coupling with the microphysical cycles of various aerosols. Observations of these clouds have accelerated in the past 20 years. Specifically, the Mars Orbiter Laser Altimeter (MOLA) on the Mars Global Surveyor (MGS) spacecraft has enabled the identification of CO_2 ice composition with several cloud detections in the troposphere below an altitude of 10 km above the surface (Caillé et al., 2023; Neumann et al., 2003). Some of these observations correspond to the polar winter periods, raising questions about the significance of CO_2 ice clouds in the formation of the seasonal polar caps by precipitation. Although Ivanov and Muhleman (2001) estimated that their overall contribution was not significant, observations from the Mars Climate Sounder (MCS) (Hu et al., 2012) instrument aboard the Mars Reconnaissance Orbiter (MRO) led Alsaeed and Hayne (2022) to estimate that up to 15% of the CO_2 ice mass in the polar caps could originate from snowfall, with a strong discrepancy between the two poles. However, it is notably difficult to observe the Martian polar night atmosphere and, consequently, this limits the analysis of the formation and evolution of these CO_2 ice clouds.

These observational challenges cannot easily be addressed by modeling, as the formation of these clouds can involve a wide range of spatial and temporal scales. Tobie et al. (2003) studied scenarios for the formation of polar

CO_2 ice clouds through atmospheric cooling induced by the propagation of gravity waves with the observational constraints that were provided by MOLA echoes. In parallel, the specific dynamics of these clouds was studied, first by Colaprete et al. (2003) using a 1D model, and then by Colaprete et al. (2008) using a 3D global climate model. However, no study has employed a model with a fine enough resolution to resolve convective motions while having a complete CO_2 microphysics scheme. We therefore present here the first study of CO_2 ice clouds using a 3D high-resolution dynamical model that can resolve convective phenomena and that incorporates CO_2 cloud microphysics. This combination allows us to study the cloud formation phases and the different nucleation pathways related to other aerosols that are present in the troposphere, as well as the cloud dynamics. The primary objective of this study is to determine the magnitude of atmospheric temperature perturbations that can lead to the formation of a CO_2 ice cloud in the polar night. At the same time, the high resolution allows us to evaluate the convective potential of the formed cloud, and how this convective potential translates into vertical motion, the characteristics of which are dependent on atmospheric parameters. We focus on clouds below 10 km of altitude, with a long term plan to reproduce CO_2 clouds observations from MOLA.

2. LES Model and Simulation Set-Up

In order to study the formation of CO_2 ice clouds in the troposphere and their convective potential, it is necessary to use a model with a fine enough resolution to resolve the largest turbulent plumes. Therefore, we conducted simulations using a Large-Eddy Simulation (LES) model, which resolves the Navier-Stokes equations at a very high resolution (Michaels & Rafkin, 2002). The model used in this study is described in Spiga and Forget (2009); Spiga et al. (2010), where the core dynamics of the Weather Research and Forecasting (WRF) model (Skamarock & Klemp, 2008) is coupled with the physical routines of the Mars Global Climate Model (MGCM) developed by the Laboratoire de Météorologie Dynamique (Forget et al., 1999).

For this study, the physics routines in the model feature the recently implemented CO_2 microphysics (Määttänen et al., 2022). The microphysical model is based on the work of Listowski et al. (2013, 2014) and was used for a large-scale MGCM study of CO_2 ice clouds from the troposphere to the mesosphere (Määttänen et al., 2022). The implementation of the CO_2 microphysics scheme was done in the same way as the implementation of a microphysical model for water (Madeleine et al., 2014; Navarro et al., 2014). The CO_2 microphysics model provides a detailed representation of the processes of formation (heterogeneous nucleation of CO_2 on dust and water ice crystals) and evolution (condensation and sublimation with feedback on atmospheric conditions) of CO_2 ice clouds. Nucleation represents the activation of condensation nuclei, which is the formation of CO_2 ice on a substrate of different nature, whether it be dust grains or water ice. This implies not only having an atmosphere supersaturated with respect to CO_2 vapor but also having a sufficiently high saturation ratio, beyond a critical threshold that depends notably on the size and the nature of the substrates. When the saturation ratio is greater than 1 but below the critical nucleation threshold, new nuclei cannot be activated, but condensation on previously formed CO_2 ice crystals can continue until the atmosphere is no longer supersaturated. Thus, triggering cloud formation implies having a temperature perturbation that would drive to a high enough saturation ratio. Compared to a simple CO_2 parameterization, our microphysical scheme calculates the nucleation probability by integrating the nucleation rates calculated over a size distribution of nuclei discretized into 100 size classes. The nucleation probability gives the fraction of the nuclei that becomes activated for CO_2 ice formation. This scheme allows us to track the activated nuclei at each time step.

Our simulations are performed on a 3D grid of $61 \times 61 \times 61$ points with a resolution of 50 m, which is the typical resolution used in LES modeling to resolve turbulent plumes caused by the convective boundary layer during the martian day (Spiga et al., 2010). The horizontal extent of the domain is therefore 3 km × 3 km, which easily accommodates the formation of a CO_2 ice cloud with a typical observed extent of about 1.5 km (Clancy et al., 2017). The model's top is set at 8 km above the surface. In some cases, boundary effects with the model top during convection could be caused by the absence of a sponge layer in the LES model, but our simulations demonstrate that our model top appears to be adequately high to avoid such effect. The choice of the model top altitude is a good compromise, it being high enough to allow the full development of the convective motion, while still being low enough to ensure a good vertical resolution. The LES model simulations are idealized: certain physical phenomena are neglected, such as clouds. Hu et al. (2012) demonstrated that cloud coverage is more extensive at the South Pole than at the North Pole, while being less sensitive to atmospheric variations such as dust storms. Therefore, we adopt a profile from the southern Martian polar night (Ls = 90°) at a latitude of 80°S. Since there is no dust exchange with the surface or the surrounding environment, column dust opacity is prescribed from

observations. The scenario used for our LES simulations corresponds to a profile representing an average Martian year without dust storms (Montabone et al., 2015). The initial CO_2 vapor mixing ratio is set to 0.95 throughout the domain, and the atmospheric temperature only varies with altitude. To ensure a temperature below the condensation point of CO_2 and initiation of CO_2 ice cloud formation, we introduce a temperature perturbation at the initial state in the center of the domain. It takes the form of an ovoid shape centered at 2,500 m altitude, with a horizontal extent of 1 km and a vertical extent of 1.8 km. As explained in more detail in Section 3.1, placing our perturbation at that altitude will allow CO_2 ice crystals to form on water ice crystals, which is particularly interesting for studying the coupling between the different aerosol cycles. This altitude is also consistent with the part of the polar troposphere that could be affected by gravity waves (Tobie et al., 2003). The temperature different ΔT between the center of the ovoid and the initial profile is a sensitivity parameter of our study. The temperature gradient between the center and the edges of the perturbation is linear. Our perturbation is instantaneous, meaning that we apply the perturbation to the initial temperature profile immediately at the first time step. Although this is a significant idealization, it allows us to study the overall effect of temperature perturbations, rather than focusing on more realistic ones resulting from gravity wave propagation (a highly probable scenario in the polar nights). A potential avenue for future improvement of the model would be to test such a wave propagation. This would result in a temperature perturbation of similar magnitude but with a different and asymmetric spatial evolution depending on the propagation direction. Typical speeds provided by Tobie et al. (2003) allow us to estimate that the propagation is sufficiently rapid for the atmospheric state to be similar to the one we simulate in our cases with horizontal background wind (see Section 4.3).

3. Lifecycle Scenario of a CO_2 Ice Cloud in the Martian Troposphere

3.1. CO_2 Ice Cloud Formation

The results presented in this section are from a simulation with an initial perturbation of $\Delta T = -2K$. According to modeling by Tobie et al. (2003), a $\Delta T = -2K$ could be caused by the propagation of a gravity wave in polar nights. Moreover, such perturbations of the order of a few degrees have also been observed in radio occultations of the troposphere by MGS (Hu et al., 2012). Some of the perturbed temperature-pressure profiles in the southern hemisphere have been associated with presence of CO_2 ice clouds when compared with MOLA observations (Hu et al., 2012). This suggests that such a small perturbation could be sufficient to trigger CO_2 condensation and ice cloud formation. One-dimensional modeling studies by Colaprete et al. (2003) demonstrated that a cloud formed under these conditions could have an important enough convective potential so that its vertical displacement is sufficiently large to be observed.

Figure 1a shows vertical temperature profiles at the center of the perturbation at different times during the early stages of the simulation. These temperature profiles show how the added cold perturbation affects the atmosphere before cloud formation, and Figure 1b shows the corresponding profiles of saturation ratio. The saturation ratio profiles particularly illustrate that within the perturbation, thermodynamic and microphysical conditions trigger the nucleation of CO_2. The temperature and pressure conditions imply a CO_2 saturation ratio above the nucleation threshold. This threshold depends on various environmental parameters and the size of the condensation nuclei, and it is explicitly calculated in our simulations by the microphysical model. Laboratory studies (Glandorf et al., 2002) provide a typical order of magnitude estimate for the polar night conditions that we indicate in Figure 1b to guide the eye. The black line on Figure 1b corresponds to a saturation profile outside the perturbation, at the southern border of the simulated domain. This shows that, while the atmosphere is supersaturated even without a cold perturbation, the saturation ratio is not high enough to allow nucleation. The condensation nuclei present within the perturbation are then "activated," meaning that the condensation of CO_2 vapor onto a substrate of another species, such as dust or ice crystals, is possible. Profiles after 10 and 18 s of simulation from Figure 1a show that phase change releases latent heat, resulting in atmospheric warming and a decrease in the saturation ratio. The region within the perturbation remains supersaturated ($S > 1$) for 18s, but saturation ratio is not high enough anymore to trigger nucleation, meaning that new nuclei can not be activated. However, condensation continues on the already activated nuclei (condensation of CO_2 vapor onto CO_2 ice). We consider that the cloud formation phase lasts as long as the perturbation area is supersaturated. This means that an estimate for the time required for complete cloud formation is 18s. Beyond this time, the saturation ratio returns to one in the cloud formation zone, and condensation ceases. It is worth noting, however, that the atmosphere remains supersaturated around the perturbation both horizontally and vertically. The cloud can thus continue to grow if it is transported to such a supersaturated zone.

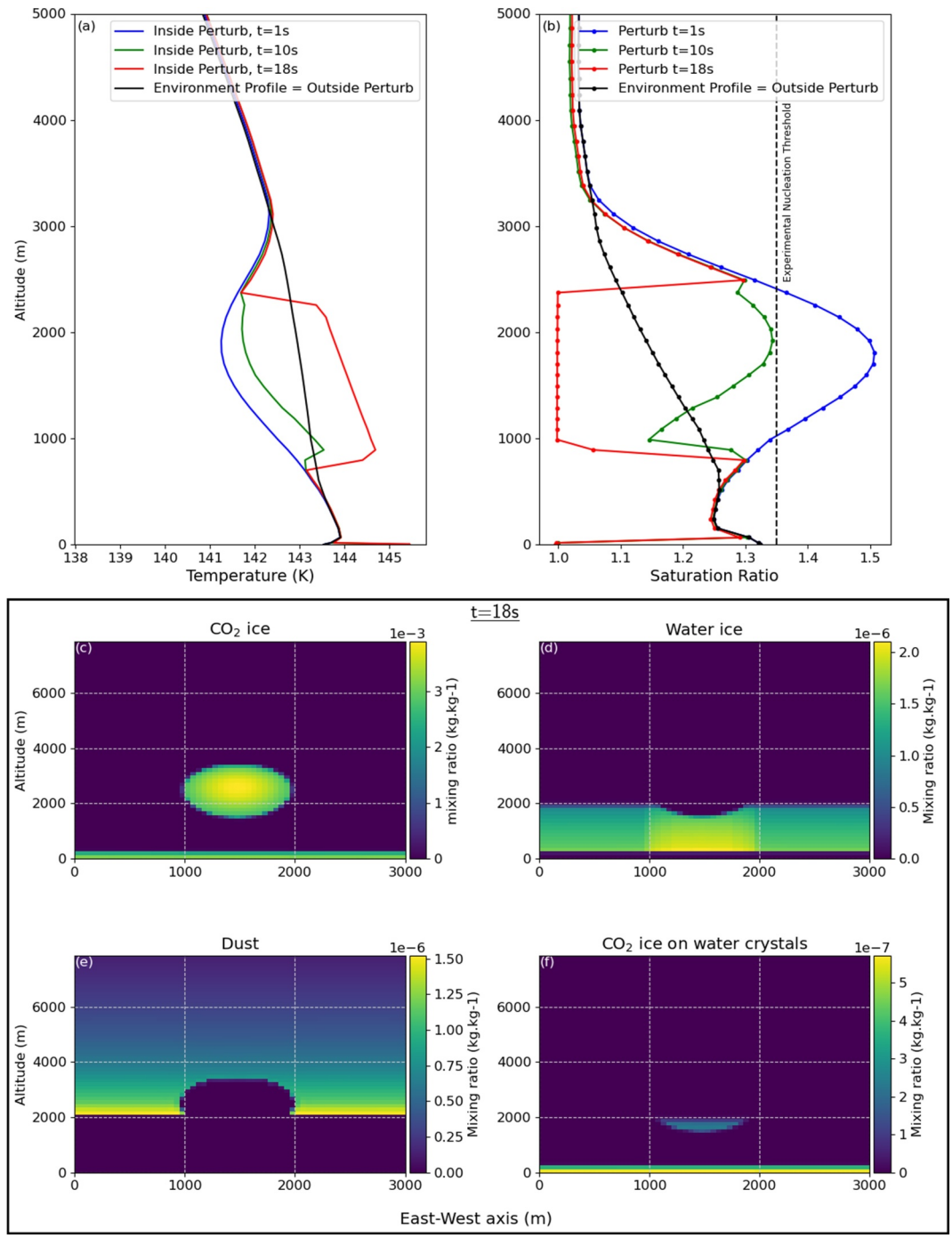

Figure 1. Formation of a CO_2 ice cloud during the first 18 s of the simulation with a -2K initial perturbation. Top panels show the evolution of the temperature (left) and the saturation ratio (right) at the center of the perturbation. Experimental nucleation threshold is only indicative as it depends on the atmospheric conditions and condensation nuclei sizes. Bottom panels show how CO_2 ice and water ice used all available dust as condensation nuclei through the mass mixing ratios of (c) CO_2 ice, (d) water ice, (e) dust and (f) water ice serving as condensation nuclei for CO_2 ice.

Figures 1c–1f provide insight into the distribution of condensation nuclei in a context where both CO_2 vapor and water vapor can condense and CO_2 ice can form onto dust and water ice crystals. At the end of the CO_2 ice cloud formation phase, all dust grains below 2000m or within the perturbation have been activated in the formation of CO_2 ice and water ice crystals. In the supersaturated regions (perturbation and the layer closest to the surface),

both cloud formation processes compete, but since water condensation is triggered first in the code, it activates the majority of the grains. In our model, CO_2 nucleation is also possible on water ice crystals. This is observed in Figure 1f, indicating that the formed CO_2 ice cloud consists of both CO_2 ice crystals formed on a dust substrate and a water ice crystal substrate. In our model, the so-called contact parameter m, that dictates how easy it is for CO2 to nucleate on a specific substrate, is fixed to be the same for dust grain and water ice crystals. This means that it is as easy to trigger nucleation in both cases, and nucleation of water ice on dust would not prevent the later formation of CO_2 ice cloud by using all the available dust, since CO_2 can also readily nucleate on water ice. In reality, the contact parameter might be initially different, but it is very likely that, in the atmosphere, dust grains absorb water molecules, leading to the formation of a thin water ice layer at their surfaces (Listowski et al., 2013; Määttänen et al., 2022). Thus, nucleating CO_2 on dust and nucleating CO_2 on water ice crystals would have similar contact parameters and require similar saturation ratio values.

3.2. Dynamics of the CO_2 Ice Cloud

The phase change of CO_2 involves the release of latent heat, resulting in atmospheric warming within the cloud, as shown in Figure 1a. This warming creates a convective potential, which can be assessed by comparing the temperature difference between the cloud interior and the surrounding environment. This potential is commonly referred to as CAPE (Convective Available Potential Energy) and is a theoretical measure of a cloud's intrinsic ability to move vertically in the atmosphere. Here, we use CAPE to compare the convective potential of clouds in our various simulations. The $\Delta T = -2K$ perturbation leads to a CAPE of 39 J kg^{-1}, which is within the range given by Colaprete et al. (2003) for the polar nights. By calculating the buoyancy force of the cloud (Colaprete et al., 2003), we obtain a theoretical maximum vertical velocity on the order of 9 m s^{-1} for our simulation. Figures 2a and 2b illustrate the evolution of winds during the stationary phase of the CO_2 ice cloud. Due to the temperature difference with the environment, the winds gradually turn upward, first beneath then within the cloud. In order for visible convection, that is, cloud displacement, to occur, the upward winds must be sufficiently strong to lift the majority of CO_2 ice crystals comprising the cloud. These crystals grow until they reach a critical size beyond which they precipitate (detailed in the following section). Thus, in our definition, the onset of convection corresponds to the moment when the vertical winds exert an upward force stronger than the weight of the crystals, meaning vertical advection starts overcoming sedimentation.

An animation tracking the cloud's evolution through the CO_2 ice mixing ratio allows us to assess the onset of its movement. We illustrate this in Figure 2e, showing temporal evolution of CO_2 ice mixing ratio at the center of the domain. The timescale for a cloud to form from a $\Delta T = -2$ K disturbance and begin ascending is of the order of 100 s. During its displacement, the maximum vertical velocity attained is $w_{max} = 8.9$ m s^{-1}, which agrees with the previously calculated theoretical value (9 m s^{-1}), indicating minimal friction and horizontal entrainment in the Martian troposphere in our simulation. This maximum velocity is reached after 400 s (see Figure 2f).

While condensation becomes possible again as the cloud encounters new supersaturated regions higher in the atmosphere, the cloud cools adiabatically (but not enough to trigger formation of a new cloud), resulting in a loss of buoyancy, thus a deceleration beyond 400 s. The top of the cloud, initially located at an altitude of 3,350 m above the surface, reaches an altitude of 5,050 m after 900 s (see Figure 2e). The cloud then enters a new stationary phase before dissipating due to the precipitation of CO_2 ice crystals (see Section 3.3).

The initial temperature gradient between the center and edges of the perturbation translates into a stronger (weaker) condensation and heating in the center (edges) of the cloud. As a result of this condensation intensity difference, the vertical wind speed is stronger below the center of the cloud. Thus, the cloud does not move uniformly, and a horizontal circulation forms at the edges of the cloud (see Figures 2c and 2d). Under the effect of these horizontal winds and the differences in speed between its different parts, the cloud undergoes deformation during its ascent. Figure 2d, in particular, shows that CO_2 ice crystals concentrate in two zones: the center of the cloud and an outer ring corresponding to the former edges of the cloud. As the cloud ascends, continuous precipitation takes place beneath it, resulting in a morphology reminiscent of terrestrial cumulonimbus clouds, that is, a columnar cloud formation with important vertical extent, as can also be seen in Figure 2d.

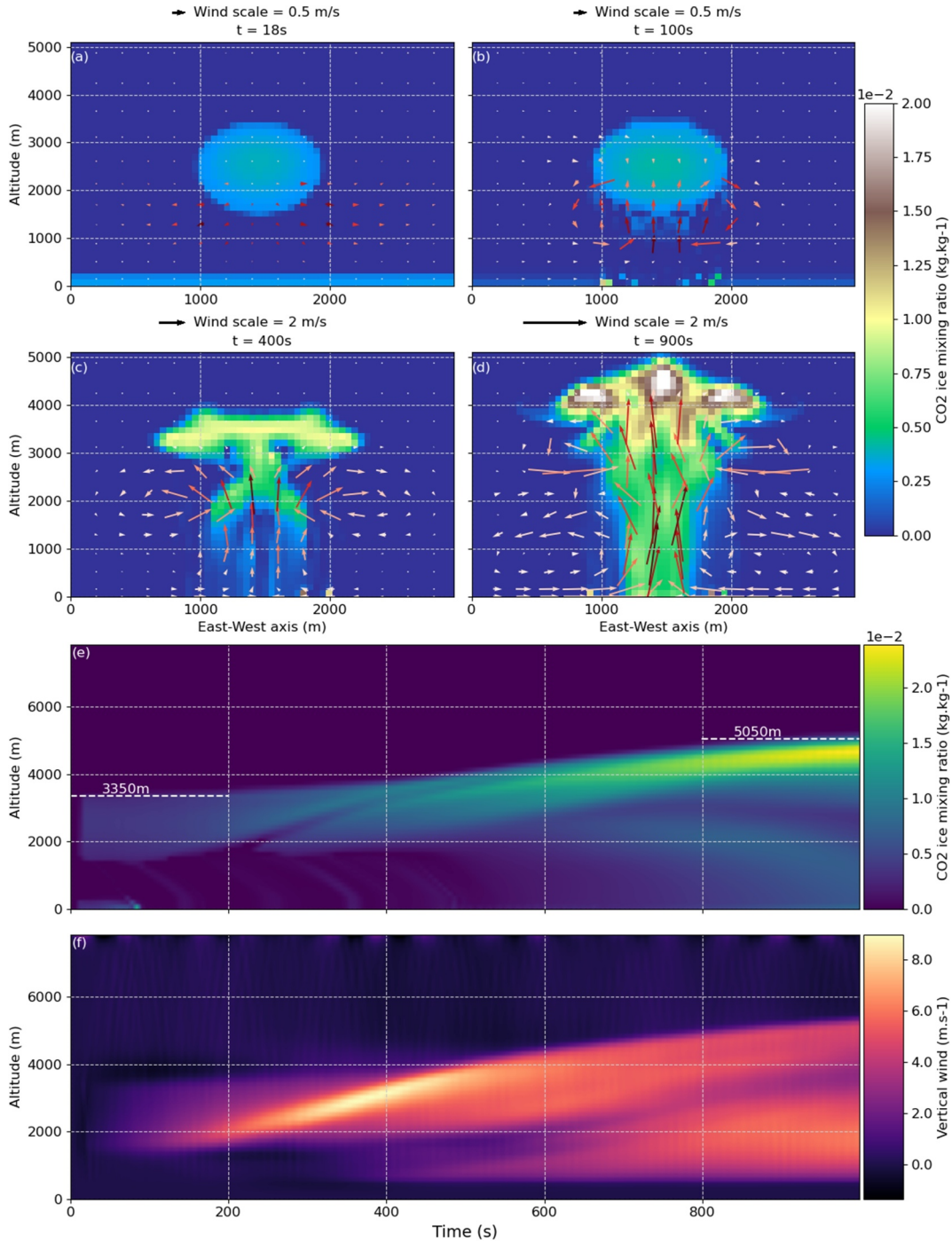

Figure 2. Convective motion of a CO_2 ice cloud. Four top panels (a–d) give wind field on CO_2 ice mixing ratio background. Arrow colors illustrate windy intensity just like arrow length. Two bottom panels are CO_2 ice mixing ratio (e) and vertical wind velocity (f) at the center of the domain, that is, cloud center, as a function of altitude and simulation time. Maximum altitude is reached by the top of the cloud after 900 s while maximum updraft velocity is reached after 400 s.

3.3. Variation of Precipitation Intensity During Cloud Ascent

Studying the life cycle of CO_2 clouds also emphasizes the investigation of precipitation processes, particularly assessing their contribution to surface interactions and potentially to the development of polar caps (P. Hayne et al., 2014). Throughout the various phases mentioned earlier, CO_2 ice crystals grow whenever condensation

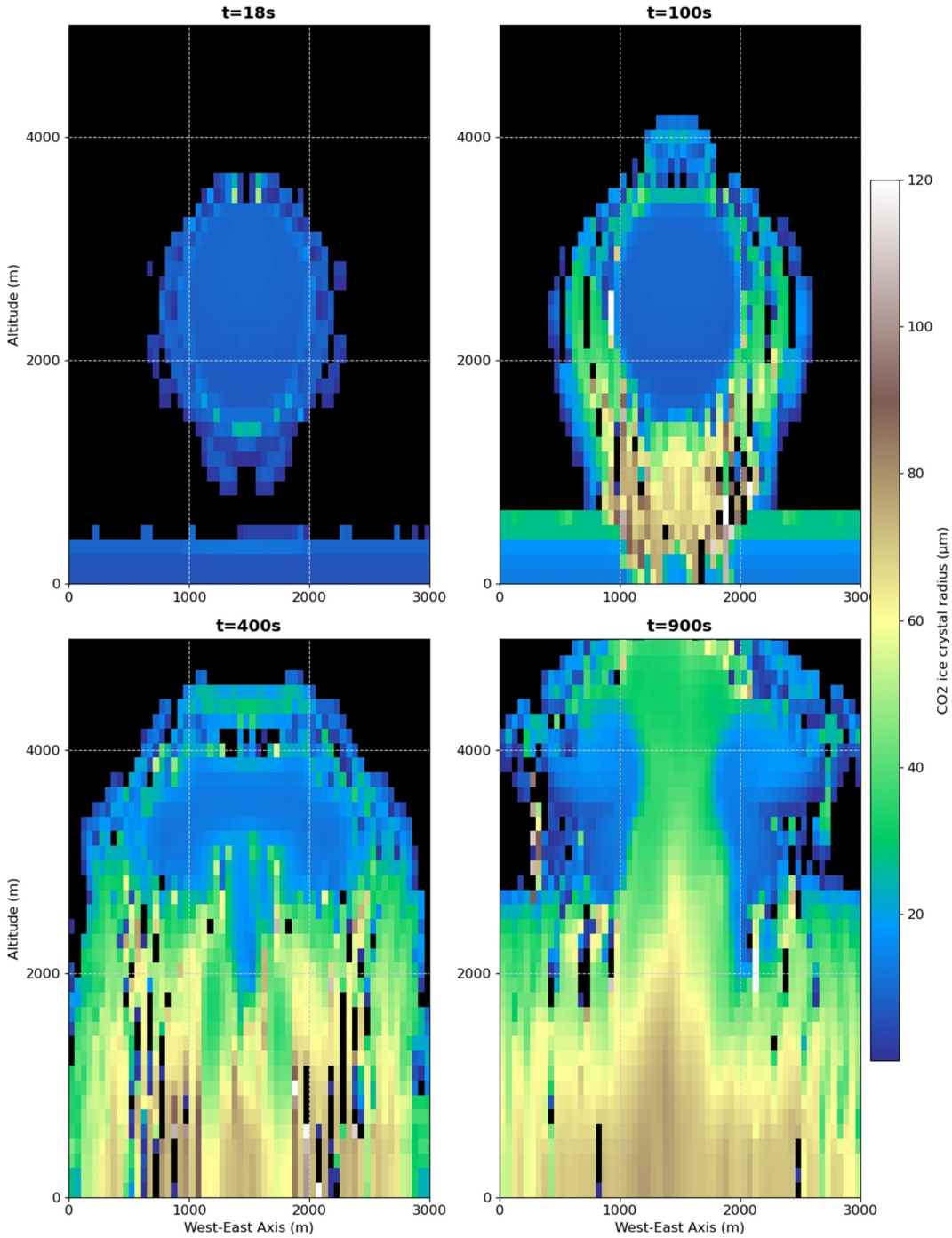

Figure 3. Development of precipitation at different times of the simulation illustrated by vertical-cross sections of CO_2 ice crystal size. The black color corresponds to a zero radius, indicating the absence of crystals. Difference with Figure 2 come from areas with very low CO_2 ice mixing ratio that do not appear clearly in Figure 2.

becomes feasible (during the cloud formation phase and again during the upward motion as they encounter new supersaturated regions). However, due to the intensity of buoyancy reached, there exists a size threshold beyond which the crystals can no longer be lifted, and thus they precipitate to the surface. Figure 3 illustrates the radii of CO_2 ice crystals at different moments during cloud ascent. Within the cloud, crystals radii seem to range from 10 to 40 microns, which is consistent with the expected crystal radii during the Martian polar night as estimated from observations (P. O. Hayne et al., 2012; P. Hayne et al., 2014; Hu et al., 2012). Figure 3 also allows tracking and

Table 1
Convection Characteristics in Each Sensitivity Test

Simulation	Alt_{max} (m)	τ_{altmax} (s)	W_{max} (m s^{-1})	τ_{Wmax} (s)
Ref simu	5,050	980	8.9	400
Delt(T) = −5	4,290	788	7.1	400
Less Dust	3,520	576	6.3	350
More Dust	5,600	1,740	7.3	436
With wind	4,300	529	5.7	400

evaluating the critical sedimentation size of CO_2 ice crystals. This critical size is the size at which the sedimentation speed of the crystal is equal to the vertical wind speed. So, when a crystal reaches a larger size than the critical size, it cannot be transported along with the rest of the cloud and sediments. Thus, this critical size obviously depends on the intensity of the vertical wind. At the beginning of the convective phase around 100s, when the wind is still weak, only crystals with sizes less than about 20 microns make up the cloud. At 400s, when the vertical velocity is at its maximum, crystals with a radius larger than 40 microns can no longer stay at a constant altitude and sediment. Finally, at 900s that is, the end of the convective phase, it is observed that all crystals in the center of the cloud have reached this limit size, indicating the onset of the cloud's dissipation.

We can also explore the sizes reached by the precipitating crystals to estimate the quantity of CO_2 ice that could potentially reach the surface. On average, the largest crystals are on the order of 100 microns (see Figure 3). Not all of these crystals make it to the surface. Upon descent, these crystals re-enter warmer regions of the troposphere where they can sublime. This sublimation highlights the significant coupling between the dynamics of CO_2 ice clouds and aerosol cycles within the troposphere. Indeed, since the CO_2 ice crystals have formed on both dust and water ice, both particle types are vertically redistributed due to the convection and sedimentation followed by CO_2 ice sublimation releasing the particles.

Although we have not specifically examined the cloud dissipation phase beyond 900 s of simulation, the simulations indicate that the cloud primarily dissipates through precipitation. When the cloud becomes stationary, condensation ceases entirely, and the upward force can no longer counterbalance the weight of the CO_2 ice crystals. Large scale temperature variation processes, such as thermal tides that are dominant at lower latitudes are minimal in the polar night. The Mars Climate Database shows that within 12 hr, at 6 km of altitude, temperatures only change by less than 0.2 K (Millour et al., 2017). During the typical timescale of our simulation, that is, around 1000s, environmental temperature changes by around 0.04 K. These minimal large-scale temperature variations imply that sublimation would be a very slow process when compared to precipitation that is a very rapid process in our simulations. Thus, it seems that sedimentation, and not sublimation, is the dominant process for the dissipation of the convective CO_2 ice clouds.

4. Sensitivity of Cloud Evolution to Atmospheric Conditions

In order to study the impact of different atmospheric conditions, as well as the characteristics of the perturbation of the initial profile, on cloud formation and the establishment of convection, we conducted several sensitivity tests. We modified the temperature of the disturbance, the initial distribution of dust in the atmosphere, and added horizontal wind shear to the profile.

The characteristics of the convection developed in each sensitivity test are presented in Table 1. The evolution of the cloud itself is illustrated by tracking the CO_2 ice mixing ratio at the center of the domain in Figure 4, showing the differences in the cloud development. It should be noted that we present only a subset of the simulations carried out to illustrate the expected impact; other simulations were also conducted, which are mentioned for each test and allowed us to verify dependencies. In the following section, the simulation (with $\Delta T = -2$ K) whose results were presented previously is referred to as the reference simulation.

4.1. Sensitivity to the Temperature of the Perturbation

The first modified parameter is the temperature of the perturbation ΔT, with three types of simulations: one simulation with a minimal cooling (on the order of $\Delta T = -1$ K, thereafter called T_{-1}), simulations with intense cooling that could potentially be justified by gravity wave propagation scenarios ($\Delta T = -5$ K and $\Delta T = -10$ K, respectively T_{-5} and T_{-10}), and an extreme simulation that investigates the model's stability at very high temperature perturbations ($\Delta T = -20$ K mentioned as T_{-20}).

When the perturbation is weak, that is, for T_{-1} or less intense perturbation, the cloud takes longer to form, condensation is less intense, and consequently, latent heat release is also reduced. As a result, the vertical winds never become strong enough to lift most of the CO_2 ice crystals, and the cloud is non-convective. In contrast, for

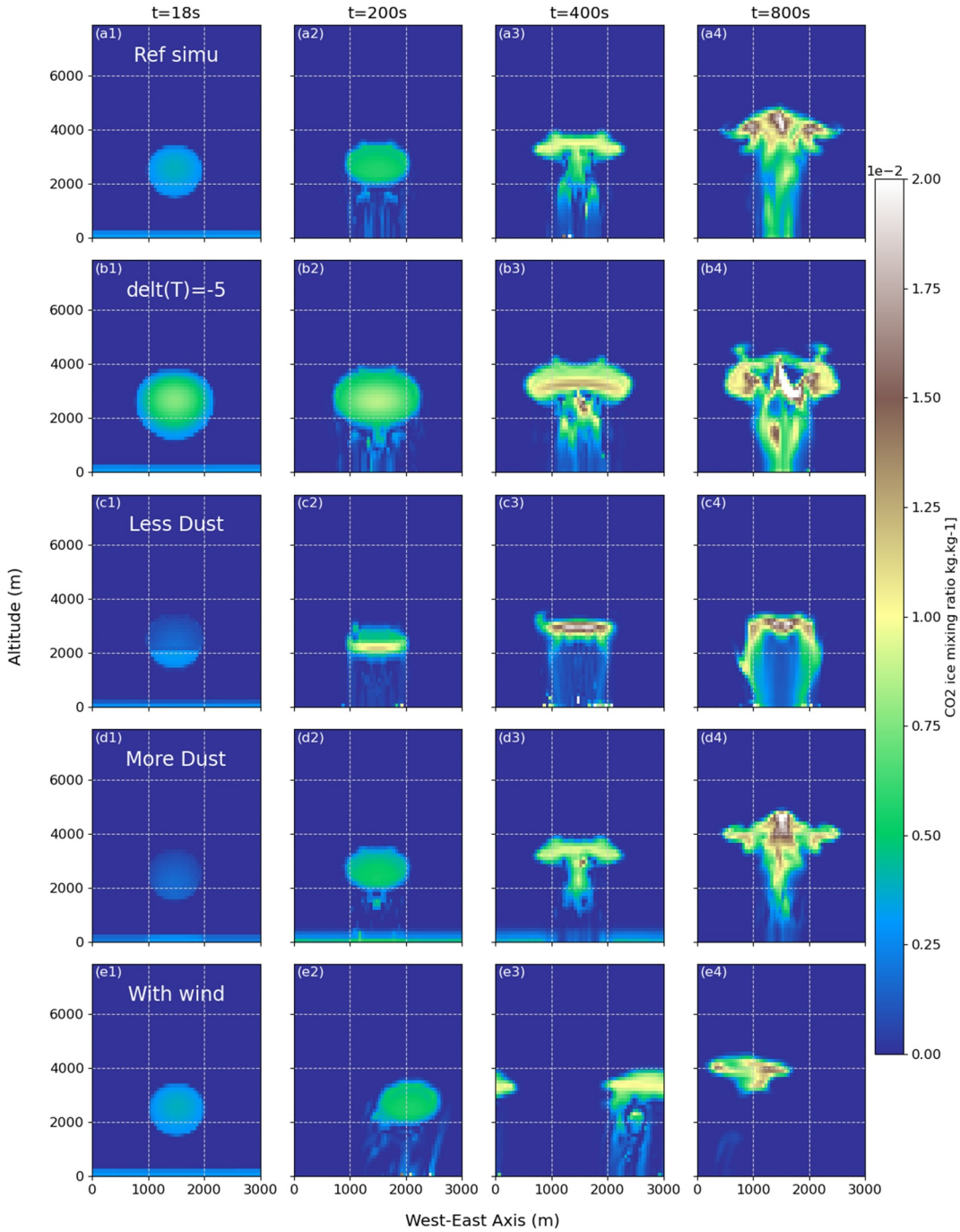

Figure 4. Deformation of the CO_2 ice cloud over time for the different sensitivity tests. Columns 1–4 correspond to vertical cross-sections at the center of the domain at 18, 200, 400, and 800s, respectively. Rows a-e correspond to the reference simulation (a), a simulation with an initial perturbation at $\Delta = -5$K (b), dust-depleted (c) and dust-enriched (d) simulations, and the simulation with horizontal winds (e).

the extreme simulations (initially on the order of −20 K or colder), condensation is initially extremely intense, and convection establishes more quickly than in the reference simulation. However, excessively strong initial condensation implies that the crystals reach the critical size for sedimentation more rapidly. Consequently, convection is triggered more quickly but is less intense (with lower maximum speed and altitude reached) and terminates much earlier. The results of T_{-20} demonstrate the impact of the initial temperature of the disturbance on convection, which is also observed more moderately for T_{-5} and T_{-10}.

The temperature of the perturbation thus plays a role in the intensity of convection rather than its initiation, as the time scales required to trigger convection and reach maximum speed are similar for each simulation. However, and perhaps counter-intuitively, the colder the perturbation, the lower the maximum attained speed (8.9 m s^{-1} for the reference simulation, 7.1 m s^{-1} for T_{-5}, and 6.0 m s^{-1} for T_{-10}). Similarly, as the maximum speed achieved is lower and CO_2 ice crystals are heavier at the end of the cloud formation phase, it results in the cloud reaching a progressively lower maximum altitude when the perturbation is colder (5,050 m for the reference simulation, 4,290 m for T_{-5}, and 4,000 m for T_{-10}). Therefore, the simulation allowing the formation of a cloud with the most significant convective potential seems to be the one that tries to mimic a fairly realistic environment with a temperature perturbation that could be triggered by the propagation of a typical gravity wave in the polar night.

4.2. Sensitivity to the Initial Dust Profile

In addition to thermodynamic conditions, it is possible to study the sensitivity to microphysical conditions by, for example, varying the number of initially available condensation nuclei. We conducted simulations with an enriched or depleted population of dust particles compared to the reference simulation while keeping the amount of CO_2 vapor and the temperature of the perturbation constant. Thus, we know that the cooling is sufficient to condense the same amount of CO_2 but onto a variable number of condensation nuclei. The initial dust profile is defined by a two-moment scheme (Madeleine et al., 2011). Given the size distribution and the number of particles, we can deduce the mass mixing ratio. Our objective is to study the effect of having less (or more) condensation nuclei, so we decrease (or increase) the number of dust particles and adjust accordingly the mass mixing ratio, ensuring that the initial grain size remains consistent across simulations, as this size plays a crucial role in the nucleation of CO_2.

Here, we present results for a simulation in which the number density of dust particles has been divided by 10 in comparison to the reference simulation, while following the same size distribution. When the initial profile is depleted of dust particles, there are fewer nuclei available for condensation, resulting in larger CO_2 ice crystals at the end of the cloud formation phase. Once again, this leads to a deceleration of convection, as heavier crystals require higher wind speeds for vertical displacement. Not only does the convection start later, it is also less intense with a maximum attained speed of only 6.3 m s^{-1}. This comes from crystals already being closer to the critical size for sedimentation at the start of the convective phase, thus having a smaller size margin before sedimentation. Since the end of the cloud vertical movement corresponds to the moment the majority of crystals reach this critical size, the convection ends sooner and the CO_2 ice cloud reaches a lower final altitude of only 3,520 m. Furthermore, since the vapor condenses onto a limited number of nuclei, all CO_2 ice crystals that are not heavy enough to sediment have a size close to the threshold size. Thus, the cloud exhibits a higher homogeneity in the CO_2 ice mixing ratio. The absence of a gradient between the cloud's center and edges results in a different cloud deformation, with a flatter shape where all parts of the cloud move at the same speed (see 4c).

Conversely, when the profile is enriched in dust, there are more grains on which CO_2 vapor can condense compared to the reference simulation. Consequently, the crystals formed during cloud formation are smaller. This means that during convection, when the cloud reaches new supersaturated area in upper atmospheric layers, condensation can resume on these crystals without them necessarily reaching the sedimentation threshold size. The characteristics of convection presented in Table 1 indeed show that convection lasts longer in this case (final altitude reached after 1,740 s when it takes 980 s in the reference simulation), allowing the cloud to reach a higher final altitude (5,600 m) while following a deformation similar to the reference simulation (see Figure 4d). These simulations notably demonstrate that an enrichment of the troposphere with dust, potentially resulting from dust storms, theoretically enables the formed CO_2 ice clouds to reach higher altitudes.

4.3. Sensitivity to Horizontal Winds

All previous simulations were conducted without horizontal winds in the initial profile to facilitate the analysis and to study the development of horizontal circulation associated with convection. We performed a simulation with an initial profile of horizontal winds with shear (wind speed increasing solely with altitude) with a wind speed of 2 m s^{-1} near surface and 4 m s^{-1} at the top of the domain. The resulting cloud is strictly identical to that of the reference simulation only for the first 18 s, both in terms of shape and in terms of CO_2 ice mass mixing ratio, indicating that the timescale for noticeable horizontal displacement of the crystals due to the wind is longer than

the timescale for nucleation and formation of the CO_2 ice cloud. As a result, the theoretical convective potential is the same for these two simulations.

However, the added horizontal winds, typical of Martian polar nights, cause the cloud to move along the west-east axis. The release of latent heat cannot accumulate within the cloud, leading to a significant deceleration of convection due to these horizontal winds. This deceleration is reflected not in a difference in the time it takes for convection to establish, but rather in a much lower maximum velocity attained (5.7 m s^{-1} with horizontal winds, 8.9 m s^{-1} without). Since the CO_2 ice crystals reach a similar size as those in the reference simulation, a lower maximum velocity logically results in a much quicker cessation of convective motion (final altitude is reached after 529 s with winds, 980 s without): with slower cloud motion, it takes longer to reach new supersaturated areas to initiate convection and trigger a renewed release of latent heat to sustain convection. Consequently, the maximum altitude reached by the cloud top is also significantly lower (4,300 m with winds, 5,050 m without).

Additionally, winds have an effect on cloud morphology. The cloud leading edge reaches new supersaturated regions first. Since the saturation ratios are not very high at higher altitudes (see Figure 1b), condensation ceases before the trailing edge of the cloud reaches the supersaturated areas. As a result, CO_2 vapor primarily condenses at the front of the cloud, causing the trailing edge of the cloud to dissipate more rapidly. This leads to a smaller cloud size and precipitation concentrated at the trailing edge of the cloud (see Figure 4e3). Considering that the propagation of a gravity wave, the preferred scenario for temperature perturbation in Martian polar nights, is generally accompanied by horizontal winds, this last simulation appears to be a first step toward a more realistic cloud simulation.

5. Conclusion

The coupling of Large Eddy Simulations (LES) and the CO_2 microphysics model provides as a powerful tool for investigating the intricate processes governing the formation and evolution of CO_2 ice clouds. By introducing a cold temperature perturbation to a Martian polar night atmospheric profile, we initiated nucleation, resulting in CO_2 ice cloud formation. The phase change induces the release of latent heat, conferring convective potential to the cloud. The ensuing vertical ascent of the cloud underscores a strong coupling between cloud dynamics and microphysics involving dust grains and water. In particular, the nucleation of CO_2 onto water ice crystals could play a crucial role in the transport of water ice at higher altitudes, when CO_2 crystals end up sublimating and releasing water. The cloud evolution leads to precipitation events that can contribute to an interaction with the surface and future simulations will help determining the contribution of CO_2 ice clouds to the evolution of polar cap.

The detailed microphysics scheme of our model allowed us to study the different pathways of nucleation and how microphysical change translates to modification of the convection properties. The modeled convective CO_2 clouds in the polar night exhibit sensitivity to atmospheric parameters, with some influencing its initiation and others determining its intensity, as observed by maximum attained speed and altitude. Notably, we established that colder perturbations inhibit proper convective development, similarly to cases where atmospheric dust was depleted or horizontal wind was present. Conversely, an enrichment of atmospheric dust, which could be induced by dust storms, significantly augments cloud dynamics in our idealized simulations. Through these tests, we can establish the maximal characteristics of convection in the troposphere, especially regarding the typical altitude range of vertical movement of a CO_2 ice cloud. In combination with gravity wave propagation modeling in polar nights, it will now be possible to determine which cloud observations can be associated with convective cloud formations in the troposphere.

These sensitivity tests pave the way toward increasingly realistic simulations that would aim at approximating the actual, observed Martian environment. While these LES-based simulations do not allow for direct comparison with observations, they constitute a pivotal step in comprehending the intricacies of CO_2 ice cloud formation and evolution. Subsequent phases of investigation could entail replacing the instantaneous temperature perturbation with an explicitly modeled gravity wave propagation. Given the potentially profound influence of dust on cloud evolution, it would be necessary to enable a more flexible, realistically evolving dust profile over time, including dust lifting from the surface.

Data Availability Statement

Model outputs for the simulations presented in this paper, as well as the code used for making the figures, are stored in the ESPRI mesocentre data repository (Caillé et al., 2024). The LES model used in this study is described in detail in Spiga et al. (2010). The CO_2 microphysics scheme is described in Määttänen et al. (2022).

Acknowledgments
We thank the Agence Nationale de la Recherche for funding (project MECCOM, ANR-18-CE31-0013) this research. Computational Resources for this project were provided through CICLAD and SPIRIT servers by the ESPRI mesocentre at the IPSL institute.

References

Alsaeed, N. R., & Hayne, P. O. (2022). Transport of water into the polar regions of mars through scavenging by co2 snowfall. *Journal of Geophysical Research: Planets*, *127*(11), e2022JE007386. https://doi.org/10.1029/2022JE007386

Caillé, V., Määttänen, A., Spiga, A., & Falletti, L. (2023). Revisiting atmospheric features of mars orbiter laser altimeter data using machine learning algorithms. *Journal of Geophysical Research: Planets*, *128*(1), e2022JE007384. https://doi.org/10.1029/2022JE007384

Caillé, V., Spiga, A., Määttänen, A., Falletti, L., & Mathé, C. (2024). Reference simulation and sensitivity tests on co2 ice cloud formation, and convection, in the martian troposphere during polar nights with a les model [dataset]. *ESPRI/IPSL*. https://doi.org/10.14768/da291f99-75d8-49a1-9f2a-62dfc7fc6790

Clancy, R. T., Montmessin, F., Benson, J., Daerden, F., Colaprete, A., & Wolff, M. J. (2017). Mars clouds. In *The atmosphere and climate of mars* (pp. 76–105). Cambridge University Press. https://doi.org/10.1017/9781139060172.005

Colaprete, A., Barnes, J., Haberle, R., & Montmessin, F. (2008). Co_2 clouds, cape and convection on mars: Observations and general circulation modeling. *Planetary and Space Science*, *56*(2), 150–180. https://doi.org/10.1016/j.pss.2007.08.010

Colaprete, A., Haberle, R. M., & Toon, O. B. (2003). Formation of convective carbon dioxide clouds near the south pole of mars. *Journal of Geophysical Research*, *108*(E7). https://doi.org/10.1029/2003JE002053

Forget, F., Hourdin, F., Fournier, R., Hourdin, C., Talagrand, O., Collins, M., et al. (1999). Improved general circulation models of the martian atmosphere from the surface to above 80 km. *Journal of Geophysical Research*, *104*(E10), 24155–24175. https://doi.org/10.1029/1999JE001025

Glandorf, D. L., Colaprete, A., Tolbert, M. A., & Toon, O. B. (2002). Co2 snow on mars and early earth: Experimental constraints. *Icarus*, *160*(1), 66–72. https://doi.org/10.1006/icar.2002.6953

Hayne, P., Paige, D., & Heavens, N. (2014). The role of snowfall in forming the seasonal ice caps of mars: Models and constraints from the mars climate sounder. *Icarus*, *231*, 122–130. https://doi.org/10.1016/j.icarus.2013.10.02003

Hayne, P. O., Paige, D. A., Schofield, J. T., Kass, D. M., Kleinböhl, A., Heavens, N. G., & McCleese, D. J. (2012). Carbon dioxide snow clouds on mars: South polar winter observations by the mars climate sounder. *Journal of Geophysical Research*, *117*(E8). https://doi.org/10.1029/2011JE004040

Hu, R., Cahoy, K., & Zuber, M. (2012). Mars atmospheric co2 condensation above the north and south poles as revealed by radio occultation, climate sounder, and laser ranging observations. *Journal of Geophysical Research (Planets)*, *117*(E7), 7002. https://doi.org/10.1029/2012JE00408707

Ivanov, A. B., & Muhleman, D. O. (2001). Cloud reflection observations: Results from the mars orbiter laser altimeter. *Icarus*, *154*(1), 190–206. https://doi.org/10.1006/icar.2001.6686

Listowski, C., Määttänen, A., Montmessin, F., Spiga, A., & Lefèvre, F. (2014). Modeling the microphysics of co2 ice clouds within wave-induced cold pockets in the martian mesosphere. *Icarus*, *237*, 239–261. https://doi.org/10.1016/j.icarus.2014.04.022

Listowski, C., Määttänen, A., Riipinen, I., Montmessin, F., & Lefèvre, F. (2013). Near-pure vapor condensation in the martian atmosphere: Co2 ice crystal growth. *Journal of Geophysical Research: Planets*, *118*(10), 2153–2171. https://doi.org/10.1002/jgre.20149

Määttänen, A., Mathé, C., Audouard, J., Listowski, C., Millour, E., Forget, F., et al. (2022). Troposphere-to-mesosphere microphysics of carbon dioxide ice clouds in a mars global climate model. *Icarus*, *385*, 115098. https://doi.org/10.1016/j.icarus.2022.115098

Madeleine, J.-B., Forget, F., Millour, E., Montabone, L., & Wolff, M. J. (2011). Revisiting the radiative impact of dust on mars using the lmd global climate model. *Journal of Geophysical Research*, *116*(E11), E11010. https://doi.org/10.1029/2011JE003855

Madeleine, J.-B., Head, J. W., Forget, F., Navarro, T., Millour, E., Spiga, A., et al. (2014). Recent ice ages on mars: The role of radiatively active clouds and cloud microphysics. *Geophysical Research Letters*, *41*(14), 4873–4879. https://doi.org/10.1002/2014GL059861

Mahaffy, P. R., Webster, C. R., Atreya, S. K., Franz, H., Wong, M., Conrad, P. G., et al. (2013). Abundance and isotopic composition of gases in the martian atmosphere from the curiosity rover. *Science*, *341*(6143), 263–266. https://doi.org/10.1126/science.1237966

Michaels, T., & Rafkin, S. (2002). Large-eddy simulation of atmospheric convection on mars. *Quarterly Journal of the Royal Meteorological Society*, *128*(599), 1–999. https://doi.org/10.1256/qj.02.169.01

Millour, E., Forget, F., Spiga, A., Vals, M., Zakharov, V., Navarro, T., & MCD/GCM Development Team (2017). The Mars climate Database (MCD version 5.3). In *Egu general assembly conference abstracts*.12247.

Montabone, L., Forget, F., Millour, E., Wilson, R., Lewis, S., Cantor, B., et al. (2015). Eight-year climatology of dust optical depth on mars. *Icarus*, *251*, 65–95. https://doi.org/10.1016/j.icarus.2014.12.034

Navarro, T., Madeleine, J.-B., Forget, F., Spiga, A., Millour, E., Montmessin, F., & Määttänen, A. (2014). Global climate modeling of the martian water cycle with improved microphysics and radiatively active water ice clouds. *Journal of Geophysical Research: Planets*, *119*(7), 1479–1495. https://doi.org/10.1002/2013JE004550

Neumann, G. A., Smith, D. E., & Zuber, M. T. (2003). Two Mars years of clouds detected by the Mars orbiter laser altimeter. *Journal of Geophysical Research (Planets)*, *108*(E4), 5023. https://doi.org/10.1029/2002JE001849

Skamarock, W. C., & Klemp, J. B. (2008). A time-split nonhydrostatic atmospheric model for weather research and forecasting applications. *Journal of Computational Physics*, *227*(7), 3465–3485. https://doi.org/10.1016/j.jcp.2007.01.037

Spiga, A., & Forget, F. (2009). A new model to simulate the martian mesoscale and microscale atmospheric circulation: Validation and first results. *Journal of Geophysical Research*, *114*(E2). https://doi.org/10.1029/2008JE003242

Spiga, A., Forget, F., Lewis, S. R., & Hinson, D. P. (2010). Structure and dynamics of the convective boundary layer on mars as inferred from large-eddy simulations and remote-sensing measurements. *Quarterly Journal of the Royal Meteorological Society*, *136*(647), 414–428. https://doi.org/10.1002/qj.563

Tobie, G., Forget, F., & Lott, F. (2003). Numerical simulation of the winter polar wave clouds observed by mars global surveyor mars orbiter laser altimeter. *Icarus*, *164*(1), 33–49. https://doi.org/10.1016/S0019-1035(03)00131-3